ELSEVIER

Journal of Nuclear Materials 283–287 (2000) 205–209

journal of nuclear materials

www.elsevier.nl/locate/jnucmat

Correlation of simulated TEM images with irradiation induced damage

R. Schäublin *, P. de Almeida, A. Almazouzi, M. Victoria

EURATOM-Association-Swiss Conf., Centre of Research in Plasma Physics, Fusion Technology Materials Group, Swiss Federal Institute of Technology, Lausanne, 5232 Villigen PSI, Switzerland

Abstract

Crystal damage induced by irradiation is investigated using transmission electron microscopy (TEM) coupled to molecular dynamics (MD) calculations. The displacement cascades are simulated for energies ranging from 10 to 50 keV in Al, Ni and Cu and for times of up to a few tens of picoseconds. Samples are then used to perform simulations of the TEM images that one could observe experimentally. Diffraction contrast is simulated using a method based on the multislice technique. It appears that the cascade induced damage in Al imaged in weak beam exhibits little contrast, which is too low to be experimentally visible, while in Ni and Cu a good contrast is observed. The number of visible clusters is always lower than the actual one. Conversely, high resolution TEM (HRTEM) imaging allows most of the defects contained in the sample to be observed, although experimental difficulties arise due to the low contrast intensity of the smallest defects. Single point defects give rise in HTREM to a contrast that is similar to that of cavities. TEM imaging of the defects is discussed in relation to the actual size of the defects and to the number of clusters deduced from MD simulations.

1. Introduction

Under cascade irradiation, low dose and temperatures below $0.3T_m$, where T_m is the melting point, the densities of defects visible in TEM are one order of magnitude smaller in Ni than in Cu [1], whereas in Al no defect has been observed [2]. The direct observation by TEM of the induced defects is however hindered by their nanometric sizes [3] that are at the limit of the resolution of the technique. Molecular dynamics (MD) numerical simulations appear in this context an appropriate technique [4] to investigate the formation of defects from the early stages of the displacement cascade. The difficulty in such studies is the lack of direct experimental confirmation because of the sample sizes which can be handled are limited by computer power, and the non-trivial relation between the defect cluster and its TEM image. Although these three metals exhibit the same crystallographic structure, they are very different in terms of melting temperature, atomic density and electron–phonon coupling. These three factors play an important role on the development of the displacement cascades and thus on the distribution of the induced defects. It has been found by MD simulation of displacement cascades that in Al [5] there is almost no intra-cascade clustering in contrast to Ni [6] or Cu [7]. The comparison between Ni and Cu leads to the fact that the cascades in Ni cooled down much more rapidly than in Cu due to the stronger electron–phonon coupling in the former [8]. There is a general agreement on the type of defect clusters that can be found in post-irradiation microstructural TEM examination when sizes are larger than about 2 nm [9–12]. It is well established that in Al, almost all the observable defects are Frank-loop type clusters [10], while in Cu the majority of the damage is composed of stacking fault tetrahedra [13].

In a previous publication [14], predefined crystalline defects were simulated using MD in order to investigate: (i) the visibility of the defect cluster in terms of image contrast, (ii) the limits to which its type can be identified by its TEM image features and (iii) the correlation between its real size and its TEM image size. Interstitial-type Frank loops in Al and SFTs in Cu were analyzed. It

* Corresponding author. Tel.: +41-56 310 4082; fax: +41-56 310 4529.

E-mail address: robin.schaeublin@psi.ch (R. Schäublin).

0022-3115/00/$ - see front matter
PII: S0022-3115(00)00340-8

appeared that a Frank loop-type cluster defect in Al would in principle be visible experimentally down to surprisingly small sizes (from two interstitials upwards), provided that sample preparation is optimized, while SFTs in Cu would be difficult to identify below a size of 19 vacancies. The main goal of the present paper is to investigate by means of TEM techniques the defect clusters generated by high-energy displacement cascades as obtained by MD simulations. The TEM images are simulated using the multislice method. The approach is applied to the case of a 10 keV cascade in Al, a 30 keV cascade in Ni and a 50 keV cascade in Cu.

2. Simulations procedure

Simulations of the high-energy displacement cascades are all carried out with the MD simulation code MDCASK which is based on the embedded-atom method (EAM) [15] and the link cell method that allows a fast neighbor search and a full parallelization. Calculations were performed on the SGI Origin2000 of the Ecole Polytechnique Fédérale de Lausanne. The interatomic potentials used in this investigation are of the EAM type [15] for Ni [16], Cu [17] and for Al [18]. All three potentials were modified following the procedure developed by Proennecke et al. [19] in order to describe properly high-energy displacement cascades. The primary knock-on atoms (PKA) that are generated in a fully relaxed matrix at 10 K for Al, 100 K for Ni and 300 K for Cu have an initial respective energy of 10, 30 and 50 keV. They are followed for 30 ps for Al and Ni and 140 ps in the case of Cu, before being dynamically quenched down to 10^{-4} K.

HRTEM images of the resulting samples are calculated using the multislice technique [20]. The diffraction contrast TEM images can also be simulated using the multislice method [14]. Basically, the sample derived from the MD simulations is cut perpendicular to the electron beam direction in slices 0.2 nm thick, 15 nm a side and containing 2000 atoms. The electron wave is propagated from one slice to the other until it goes out of the sample and forms the image. The diffraction condition is selected by the beam direction. The HRTEM simulations were performed for a [0 0 1] zone axis, at 200 kV, a spherical aberration of 1.4 mm, a defocus spread of 10 nm and a beam semi-convergence of 1 mrad. The weak beam [21] condition for all cases is $\mathbf{g}$ (3.1$\mathbf{g}$), $\mathbf{g} = (2\,0\,0)$, with 200 kV electrons along [0 1 5]. Simulations are performed with the EMS software [22].

3. Results and discussion

Fig. 1 shows for Al the projection of the damage distribution (vacancies and interstitials) resulting from the MD simulation of a 10 keV cascade and the corresponding TEM simulated images. The HRTEM images obtained with various defoci values (Figs. 1(b), (c) and 2(d)) show contrasts that correspond to almost all defects that are visible on Fig. 1(a). This spatial relationship is further strengthened, Fig. 1(b) and (c), when defoci values are different from Scherzer (Fig. 1(d)). The latter brings a relatively strong contrast arising from the lattice image that swamps the information originating from the lattice defects. This fact indicates that HRTEM could be useful in the investigation of radiation damage, and more generally of small crystal defects, provided that defoci values giving a strong lattice image contrast are avoided. Moreover, the contrast features of some of the smallest vacancy and interstitial clusters outlined on Fig. 1(a) resemble the ones of a cavity [23], which can show a reversal of contrast when going from a defocus value (Fig. 1(b)) to another (Fig. 1(c)). It appears that HRTEM could be used in the identification of much smaller defect cluster than the ones resolvable in CTEM.

The $\mathbf{g}$ (3.1$\mathbf{g}$) weak beam image of the cascade in Al, Fig. 1(f), shows features that resembles Ashby–Brown contrasts [24]. It should be noted that the printed contrast of the image is enhanced in order to present all the information contained in the image. Experimentally however, only the contrast that is at the top of the image would be strong enough to be visible. There is one cluster containing two vacancies and one cluster containing five interstitials. The rest of the cascade-induced damage is composed of point defects. The single strong white contrast relates to the 5-interstitial cluster. This indicates that experimentally the damage will be hardly visible, contrary to the cases of Ni and Cu that are presented in the following.

As in Al, Ni (Fig. 2) and Cu (Fig. 3) show a good spatial correspondence between the contrast features of the HRTEM images for the two different defoci values chosen here (Figs. 2(b) and (c) and Figs. 3(b) and (c), resp.), and the defect clusters outlined on Figs. 2(a) and 3(a), respectively. It appears also that high resolution imaging using defoci values different from the Scherzer one could be appropriate to outline point defects (Fig. 2(d) and 3(d), respectively). The cavity-like contrast is however lower than in Al.

The $\mathbf{g}$(3.1$\mathbf{g}$) and $\mathbf{g}$(5.1$\mathbf{g}$) weak beam image of the cascade in respectively, Ni and in Cu (Fig. 2(f) and 3(d)) shows features that resemble Ashby–Brown contrasts. The contrast is clearer in both Ni and Cu than in the case of Al. In Ni, the weak beam image shows two white contrast features related to defect clusters that contain 5 and 10 interstitials (from left to right, respectively) visible on Fig. 2(e). The Cu $\mathbf{g}$(5.1$\mathbf{g}$) weak beam image (Fig. 3(f)) shows three white contrasts that could be believed to originate from three separate clusters. The white top contrast relates to a 27-vacancy cluster, while the bottom one relates to a 15-interstitial cluster. The white

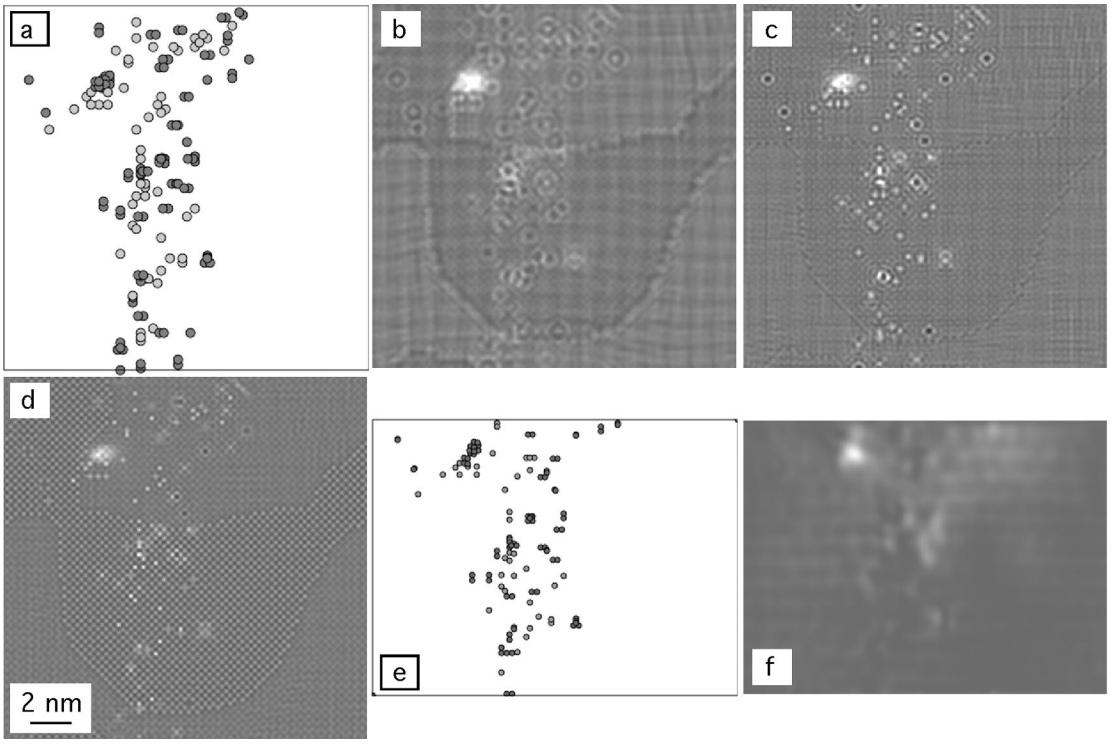

Fig. 1. MD simulated 10 keV cascade in Al. (a) Projection of vacancy (light symbol) and interstitials (dark symbol) on the plane of the TEM picture ([0 0 1] projection). Simulated HRTEM image for a defocus of (b) −40 nm and (c) 40 nm, and (d) for Scherzer defocus. (e) Projection of the defects in the electron beam direction used for the simulated weak beam image (f), with $\mathbf{g}(3.1\mathbf{g})$, $\mathbf{g} = (2\,0\,0)$, 200 kV.

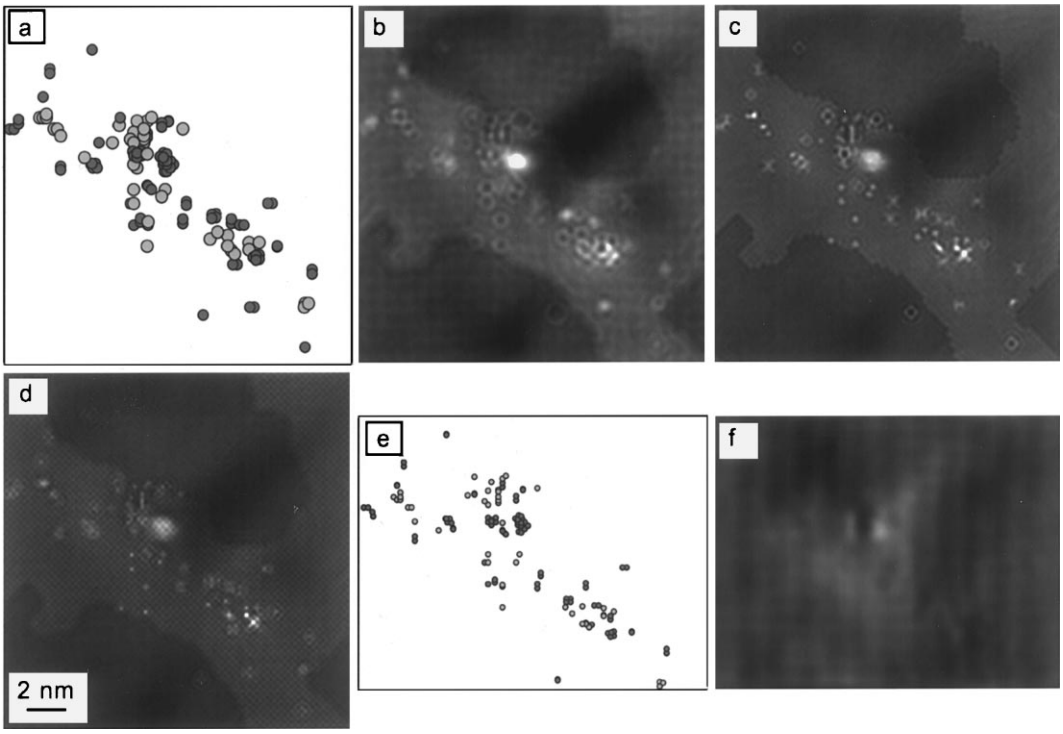

Fig. 2. MD simulated 30 keV cascade in Ni. Same caption as in Fig. 1.

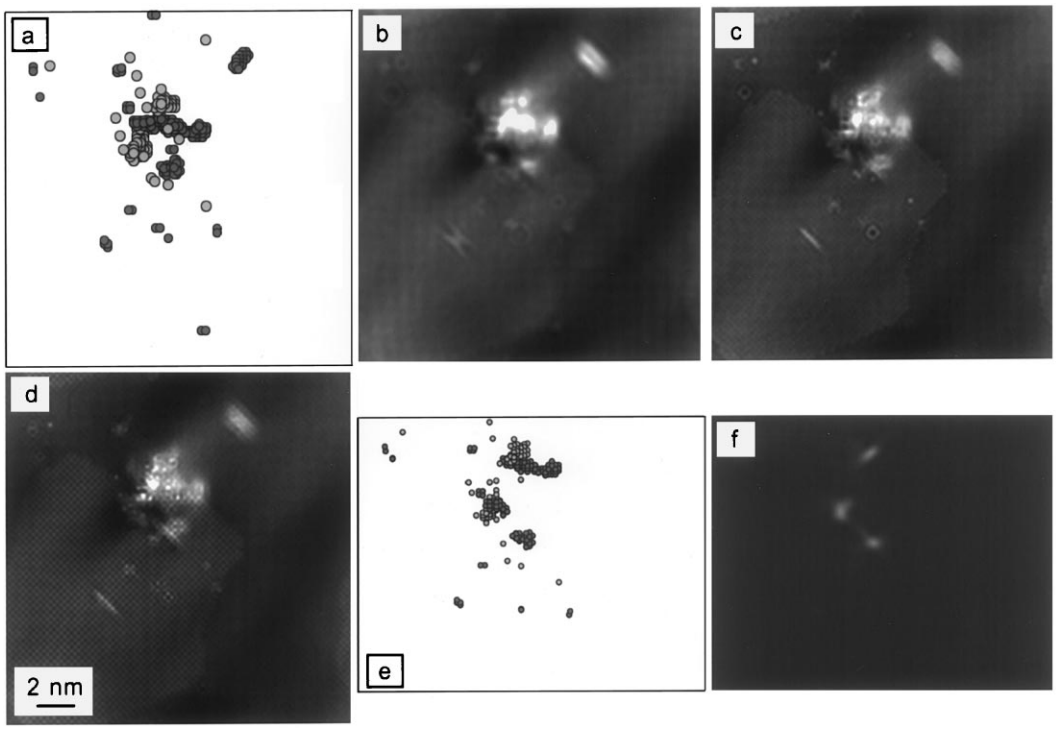

Fig. 3. MD simulated 50 keV cascade in Cu. Same caption as in Fig. 1.

contrast in the middle position arises where two separate clusters align vertically, which contain 13 and 32 vacancies. This fact shows that not only smaller clusters are lost in the TEM investigation, but, as expected, also the ones that overlap. In addition, some clusters are not visible because of the thickness contrast oscillation, as the large one visible on Fig. 3(e) on the top right that contains 40 interstitials. This could in principle be experimentally overcome by using a higher beam convergence [25].

In the following the weak beam imaging is analyzed in relation with the size and number of clusters induced by the MD simulated cascade. It appears that in Al the 10 keV cascade induces a total number of 61 Frenkel pairs. There are three clusters, two with two vacancies and one with five interstitials. Isolated point defects make the rest of the damage. It appears that most of the damage is certainly invisible on the experimental weak beam image, with only the 5-interstitial cluster visible. In Ni the 30 keV cascade induces 46 Frenkel pairs. There is one cluster with five interstitials and one cluster with 10 interstitials. The rest of the damage is composed of either clusters smaller than 3 point defects or individual point defects. Only the two larger clusters would be experimentally visible. In Cu the 50 keV cascade induces 93 Frenkel pairs. There are clusters with 13, 19, 27 vacancies and 15 and 40 interstitials. The rest of the damage is isolated point defects or clusters containing less than 5 point defects. The larger clusters would in principle be visible experimentally, of which however only three are visible. Note that the type of clusters, whether vacancy-type or interstitial-type, will be investigated at a latter stage of the study.

As pointed out earlier [14], for small sizes the Frank-loop type cluster cannot be distinguished from unorganized three-dimensional interstitial clusters for sizes smaller than about 10 interstitials or 1 nm in equivalent diameter. For larger sizes the image size increases with increasing size of the cluster. The contrasts observed in this study that are related to clusters have sizes that are about 1 nm, irrespective of the weak beam condition or the material. It appears that, on the one hand, it is not possible to use these contrasts to identify the type of clusters and, on the other hand, there is a large variation between the image size and the real size. For instance, in Cu the image of the 15-interstitial cluster would give according to Schäublin et al. [14] a cluster size of 10 interstitials when the cluster is supposed to be a Frank-loop type defect. Considering the case of Al, it can be deduced that the white contrast, which is 1 nm in size, contains 10 interstitials, or point defects. This represents less than 10% of the actual damage (122 point defects). In the case of Ni the damage deduced from the weak image represents about 20% of the actual damage. In Cu, it can be deduced from the three white 1 nm contrasts that the damage induced by the cascade is com-

posed of 30 point defects, which represent about 15% of the actual number of point defects.

4. Conclusions

It appears that in Al a 10 keV cascade induces diluted damage that will be difficult, if not impossible, to be observed experimentally using weak beam imaging. In Ni the 30 keV cascade induces a number of defects with some clusters 10 interstitials or less in size, which could in principle be observed experimentally. The 50 keV cascade in Cu induces larger clusters than in Al and Ni with sizes up to 40 interstitials, which would also be visible. However, many of the clusters and all the individual point defects remain invisible in the weak beam image acquired from the three metals. The damage inferred from the weak beam image is less than 20% of the actual damage in all three metals.

It appears that high resolution imaging using defocus values different from the ones giving a strong lattice image might be used to visualize a larger fraction of the radiation induced defects than that observed with the weak beam technique. Individual point defects exhibit contrast in simulated high resolution TEM images.

Acknowledgements

EURATOM association and the Swiss National Science Foundation are thanked for financial support. Professor P. Stadelmann of the center of electron microscopy of the EPFL is gratefully acknowledged for his continuous support.

References

[1] M.A. Kirk, I.M. Robertson, J.S. Vetrano, M.L. Jenkins, L.L. Funk, in: F.H. Garner, N.H. Packan, A.S. Kumar (Eds.), Radiation-Induced Changes in Microstructure, Proceedings of the 13th International Symposium of the ASTM, STP 955, Philadephia, 1987, p. 48.
[2] M. Kiritani, J. Nucl. Mater. 276 (2000) 41.
[3] R.S. Averback, D.N. Seidman, Mater. Sci. Forum 15–18 (1987) 963.
[4] D.J. Bacon, T. Diaz de la Rubia, J. Nucl. Mater. 216 (1994) 275.
[5] A. Almazouzi, M.J. Caturla, M. Alurralde, T. Diaz de la Rubia, M. Victoria, Nucl. Instrum. and Meth. B 153 (1999) 105.
[6] A. Almazouzi, M.J. Caturla, T. Diaz de la Rubia, M. Victoria, in: S.J. Zinkle, G.E. Lucas, R.C. Ewing, J.S. Williams (Eds.), Mater. Res. Soc. Symp. Proc., 1999, p. 685.
[7] T. Diaz de la Rubia, M.W. Guinan, Phys. Rev. B 174 (1990) 151.
[8] C.P. Flynn, R.S. Averback, Phys. Rev. B 38 (1988) 7118.
[9] M. Rühle, Radiation Damage in Reactor Materials, vol. 1, International Atomic Energy Agency, 1969, p. 113.
[10] B.L. Eyre, J. Phys. F 3 (1973) 422.
[11] M. Kiritani, J. Nucl. Mater. 133&134 (1985) 85.
[12] M.L. Jenkins, J. Nucl. Mater. 216 (1994) 124.
[13] Y. Dai, M. Victoria, Acta. Metall. 45 (1997) 3495.
[14] R. Schäublin, A. Almazouzi, Y. Dai, Y. Osetsky, M. Victoria, J. Nucl. Mater. 276 (2000) 251.
[15] M. Daw, M.I. Baskes, Phys. Rev. B 29 (12) (1984) 6443.
[16] R. Cleri, V. Rosato, Phys. Rev. B 48 (1993) 22.
[17] M. Foiles, M.I. Baskes, M.S. Daw, Phys. Rev. B 33 (1986) 7983.
[18] F. Ercolessi, J.B. Adams, Europhys. Lett. 26 (1994) 883.
[19] S. Proennecke, A. Caro, M. Victoria, T. Diaz de la Rubia, M.W. Guinan, J. Mater. Res. 6 (1991) 483.
[20] J.M. Cowley, A.F. Moodie, Acta Crystallogr. 10 (1957) 609.
[21] D.J.H. Cockayne, I.L.F. Ray, M.J. Whelan, Philos. Mag. A 20 (1969) 1265.
[22] P.A. Stadelmann, Ultramicroscopy 21 (1987) 131.
[23] M. Rühle, M. Wilkens, Cryst. Lattice Def. 6 (1975) 129.
[24] M.F. Ashby, L.M. Brown, Philos. Mag. 8 (1963) 1083.
[25] R. Schäublin, X. Meng, W.M. Stobbs, Ultramicroscopy 83 (2000) 145.